



# Carbonatite metasomatism overprinted by silicate melt metasomatism in the mantle beneath the West Eifel volcanic field

Beatrice E. Bromley<sup>1</sup>, Shuai Ma<sup>1,2</sup>, and Cliff S. J. Shaw<sup>1</sup>

<sup>1</sup>Department of Earth Sciences, University of New Brunswick, Fredericton, NB, E3B 5A3, Canada

<sup>2</sup>School of Biological, Earth and Environmental Sciences, Distillery Fields, North Mall,  
University College Cork, Cork, T23 N73K, Ireland

**Correspondence:** Cliff S. J. Shaw (cshaw@unb.ca)

Received: 4 October 2024 – Revised: 17 March 2025 – Accepted: 28 March 2025 – Published: 30 June 2025

**Abstract.** The texture and mineral compositions of mantle xenoliths from the West Eifel volcanic field (WEVF) reveal three distinct mantle events. The first, identified in LREE-depleted and isotopically depleted anhydrous (type Ib) xenoliths, resulted from partial melting of fertile mantle around 2 Ga. The second event, marked by the formation of Ti-poor, LREE-rich clinopyroxene, amphibole, and phlogopite in hydrous type Ia xenoliths, is attributed to mantle metasomatism. The third event, evidenced by LREE-depleted and MREE-enriched clinopyroxene in olivine–clinopyroxenite veins and in more evolved hornblendite and phlogopite–clinopyroxenite veins that occur in type Ia xenoliths, is associated with the passage of primitive alkaline mafic magma related to the Quaternary host magmatism.

Previous studies of mantle xenoliths have proposed that metasomatic agents could include both silicate and carbonatite melts. The trace element signatures in the studied xenoliths, particularly the Ti / Eu and  $La_N / Yb_N$  ratios and the large negative Zr and Hf anomalies, support the involvement of carbonatite melts in the formation of Ti-poor, LREE-enriched clinopyroxene and amphibole in type Ia xenoliths and clinopyroxene–amphibole–phlogopite veins in the earlier metasomatic event. The subsequent silicate melt metasomatism overprinted this carbonatite metasomatism, producing Ti-rich clinopyroxene and amphibole.

Trace element data and diffusion modelling suggest that the silicate metasomatism was not uniformly distributed, resulting in compositional heterogeneity in individual grains and xenoliths. Diffusion-controlled mixing between the earlier carbonatite-associated clinopyroxene and the silicate melt equilibrium phase is proposed to explain this heterogeneity. The complex interplay of metasomatic agents resulted in highly heterogeneous mantle compositions on a grain-to-grain and xenolith-to-xenolith scale.

## 1 Introduction

Partial melting of primitive mantle lherzolite and the attendant depletion of clinopyroxene result in partitioning of incompatible trace elements into the melt phase, leaving a refractory harzburgite–dunite residue (Bernstein et al., 2007). Many lithospheric mantle xenolith samples found worldwide show trace element and isotopic evidence of such depletion (Witt-Eickschen and Kramm, 1998; Neumann et al., 2002; Rivalenti et al., 2004). However, in some cases these isotopically depleted mantle xenoliths also contain incompatible

element-enriched phases, such as clinopyroxene, amphibole, and phlogopite, which must have been added to the mantle after the melting event. Addition of these phases occurs via mantle metasomatism. A common mechanism involved in metasomatic mineral growth, in particular of clinopyroxene, is reaction of orthopyroxene with an orthopyroxene-undersaturated melt/fluid, resulting in formation of secondary olivine and clinopyroxene. This causes transformation of lherzolite/harzburgite to wehrlite (e.g., Ionov et al., 1993; Shaw, 1999; Ionov et al., 2005; Shaw et al., 2018; Wang et al., 2018; Hauzenberger et al., 2024).

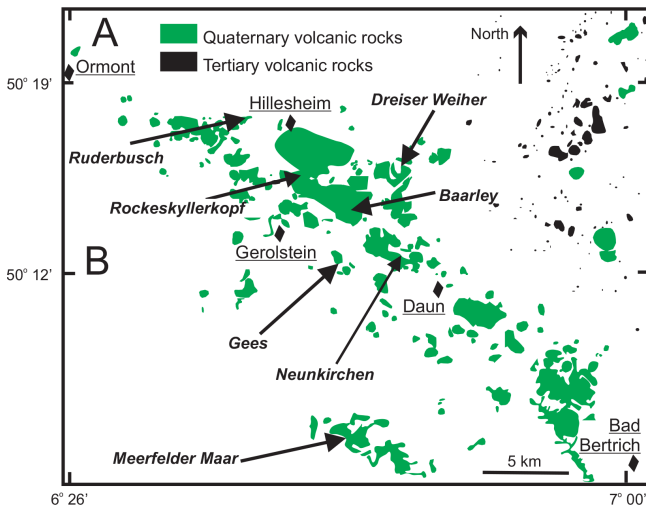


**Figure 1.** Geology of the West Eifel volcanic field (modified after Büchel, 1994) and location of the xenoliths used in this study.

Experimental studies and thermodynamic modelling indicate that wehrlite can be formed by peridotite reaction with either (1) silica-undersaturated silicate melt (Tursack and Liang, 2012; Ma and Shaw, 2022) or (2) carbonatitic melt (Klemme et al., 1995; Gervasoni et al., 2017). The trace element characteristics of wehrlite and its constituent minerals, particularly clinopyroxene, are strongly dependent on the nature of the reacting melt (Rudnick et al., 1993; Coltorti et al., 1999), as there is a strong depletion in Hf, Zr, Ti, Ta, and Al and enrichment in LREE in carbonatite melts compared to silica-undersaturated melts (Martin et al., 2013).

Wehrlitic mantle xenoliths are common in the lavas of the Quaternary West Eifel volcanic field (Fig. 1). A large proportion of these have been related to metasomatism of lherzolite and harzburgite by silicate melts related to the Quaternary volcanism; however, there is a suite of wehrlites and other peridotite lithologies for which the nature of the metasomatic agent has not yet been deciphered (Shaw et al., 2005, 2018; Ma and Shaw, 2022). In this study, we examine xenoliths from two previously unstudied locations, and we provide additional analyses of clinopyroxene from previously documented locations, together with a compilation of literature data. Our goals are the following:

1. Examine the distribution and types of metasomatism in mantle beneath the West Eifel.
2. Determine the nature of the agents of metasomatism responsible for the two metasomatic events.

## 2 Geology of the West Eifel volcanic field

Quaternary intraplate mafic alkaline volcanism in the WEVF began around 940 ka, and the last eruption occurred at

9588 BP (Mertes and Schmincke, 1983; Zolitschka et al., 1995). The northwest–southeast trending field comprises approximately 240 eruptive centres (Fig. 1) that erupted silica-undersaturated lavas as flows, tuff rings, and scoria cones. Mertes and Schmincke (1985) defined two compositional groups: the dominant suite, termed F-suite lavas, comprises leucitites, nephelinites, and melilite-bearing lavas. The second suite, comprising olivine–nephelinite and basanite (ONB suite), is younger and found mainly in the SE part of the field. Shaw and Woodland (2011) and Mertz et al. (2015) showed that the Eifel lavas were generated by melting of asthenospheric garnet peridotite and were modified by interaction with lithospheric mantle during ascent.

The lithospheric mantle below the Eifel region lies between the Moho at 28 km and the lithosphere–asthenosphere boundary at  $41 \pm 5$  km (Mertz et al., 2015, and references therein). Geophysical studies suggest that there is still magma present in the sub-Eifel mantle (Dahm et al., 2020; Eickhoff et al., 2024) so that the field cannot be considered extinct.

Previous studies of mantle xenoliths have focused on Meerfelder Maar (MFM) and Dreiser Weiher (DW) (Stosch and Seck, 1980; Stosch and Lugmair, 1986; Witt-Eickschen et al., 1993, 1998; Witt-Eickschen and Kramm, 1998; Witt-Eickschen et al., 2003), with several other studies investigating xenoliths from Gees (Lloyd et al., 1991; Zinngrebe and Foley, 1995; Rizzo et al., 2021) and Rockeskyllerkopf (Shaw et al., 2018). These locations are shown in Fig. 1.

## 3 Samples

Previous studies of mantle xenoliths from the Eifel (Witt-Eickschen et al., 1993, 1998; Witt-Eickschen and Kramm, 1998) have suggested that there is evidence of two metasomatic events in the West Eifel subcontinental lithospheric mantle (SCLM). To examine the similarities and differences between these events and their distribution across the region, we compiled literature data from the GeoRoc database (<https://georoc.eu/georoc/new-start.asp>, last access: 18 December 2022) using only samples for which both major and trace element data are available (Tables 1 and S1 in the Supplement). Since the trace element data for the Gees and Baarley localities are limited, we selected six additional samples with disseminated clinopyroxene and hydrous phases for analysis. In addition, we analyzed clinopyroxene in samples from two previously unstudied xenolith localities: Neunkirchen and Ruderbusch (Fig. 1, Table 1).

## 4 Analytical methods

The major element compositions of the minerals in sample MFM-V, a composite xenolith with a clinopyroxene–amphibole–phlogopite (CAP) vein in a lherzolite host (Fig. 2a), were determined using the Cameca SX50 elec-

**Table 1.** Summary of petrography of the Eifel xenoliths (CAP, clinopyroxene–amphibole–phlogopite; PC, phlogopite–clinopyroxene).

Type	Minerals	Reference	Event	Evidence from Cpx*
Anhydrous type Ib	Ol, opx, cpx, sp	Stosch and Lugmair (1986)	Partial melting	Strong LREE and isotopic enrichment
Hydrous type Ia CAP veins	Ol, opx, cpx, sp, amph, phlog, glass	Stosch and Lugmair (1986), Shaw and Klügel (2002)	Metasomatism 1 (carbonatite)	Strong LREE enrichment, low Ti / Eu, high xMg and Sr. Negative Zr, Hf, and Ti anomalies
Olivine clinopyroxenite	Ol, cpx	Witt-Eickschen and Kramm (1998)	Metasomatism 2 (silicate melt)	Slight LREE and isotopic enrichment, high xMg and Ti rich
Hornblendite	Amph	Witt-Eickschen et al. (1998)	Metasomatism 2 (silicate melt)	LREE enriched, Ti rich, isotopically enriched
PC veins	Cpx, phlog	Shaw et al. (2005, 2018)	Metasomatism 2 (silicate melt)	LREE enriched, Ti rich; Zr, Hf, and Ti negative anomalies small to absent

\* In the hornblendite veins, the geochemical evidence of the event association is from amphibole rather than clinopyroxene.

tron microprobe at the Bayerisches Geoinstitut, University of Bayreuth. The operating conditions were 15 kV accelerating voltage and 10 nA beam current with 30 s count time on peaks and 15 s on each background. The instrument was standardized with a variety of natural minerals and pure elements. Data reduction was done via the PAP procedure (Pouchou and Pichoir, 1984). Precision is estimated to be approximately 3 % based on repeated analyses of standards. The new samples from Gees, Baarley, Ruderbusch, and Neunkirchen were analyzed using the JEOL 6400 SEM and the EDAX genesis EDS system at the University of New Brunswick. Operating conditions were 15 kV accelerating voltage with a beam current of 5 nA. The instrument was calibrated using repeated analyses of a diopside standard, which gives a precision of ~ 5 % for all analyzed elements. A full list of major and trace element data for all new samples is presented in Table 1.

Trace element data on all samples were collected using the Australian Scientific Instruments M-50 193 nm excimer laser system coupled to the Agilent 7700x ICP-MS at the University of New Brunswick. On-sample energy, laser-firing rate, and beam size were set to 3 J cm<sup>-2</sup>, 3 Hz, and 24–33 μm respectively. Each sample was ablated for 30 s followed by a gas background of 30 s. Samples were bracketed by two standards – NIST610 and NIST620. The data were reduced using Iolite 4 software with the Trace Elements data reduction scheme (Paton et al., 2011). Precision and accuracy are estimated at 5 % based on repeated measurements of NIST610.

Literature data with trace elements were downloaded from the GeoRoc database. The data and sources are listed in Table S1.

## 5 Petrography

The peridotite xenoliths from the WEVF have been divided into two groups based on mineralogy and mineral compositions (Stosch and Seck, 1980). Amphibole- and phlogopite-free xenoliths are termed type Ib, whereas xenoliths with disseminated hydrous phases are termed type Ia. Both types may contain cross-cutting veins with associated wehrlite reaction zones, e.g., those described by Witt-Eickschen et al. (1998), Shaw et al. (2005), and Shaw et al. (2018) and shown in Fig. 2b. These types are described in more detail below.

### 5.1 Type 1a (hydrous) xenoliths

These are tabular, recrystallized peridotites with amphibole, or its breakdown products (Shaw and Klügel, 2002), as well as phlogopite (Table 1). They are found at all locations across the West Eifel. They range from phlogopite wehrlite to harzburgite. In harzburgite, orthopyroxene is porphyroclastic and is partly replaced by aggregates of olivine and clinopyroxene (Fig. 2c). Clinopyroxene close to these reaction zones commonly shows a sieve texture (Fig. 2d). The lherzolite and wehrlite xenoliths are relatively poor in orthopyroxene but contain numerous regions in which rounded olivine is intergrown with greenish clinopyroxene, suggesting its former presence. Phlogopite is present in all samples as an interstitial phase often associated with the olivine–clinopyroxene domains but also along grain boundaries of coarse-grained, deformed olivine. Phlogopite commonly has spinel aggregates in its core. Amphibole is absent in all the new samples examined, but it is present in many of the samples described in the literature, particularly those from Meerfelder Maar.

**Table 2.** Representative compositions of clinopyroxene from this study (PC, phlogopite–clinopyroxenite veins and wehrlite; Ia, type Ia xenoliths; CAP, clinopyroxene–amphibole–phlogopite veins).

Sample	96G3	96G5	96G6	98HW1	98HW3	98HW3	98MF01
Site	Gees	Gees	Gees	Gees	Gees	Gees	Meerfeld
Type	PC	PC	Ia	PC	PC	Ia	Ia
SiO <sub>2</sub>	50.93	51.19	54.88	52.97	54.49	54.71	52.44
TiO <sub>2</sub>	1.24	0.4	0.07	0	0.25	0	0.63
Al <sub>2</sub> O <sub>3</sub>	4.86	3.39	0.99	2.31	1.82	1.7	3.76
FeO	5.28	5.04	3.23	4.76	4.34	4.96	3.67
MnO	0.29	0.19	0.08	0.14	0.37	0.26	0.05
MgO	14.92	15.31	17.77	15.95	17.03	16.64	16.04
CaO	23.26	22.78	21.72	22.96	21.92	20.61	22.04
Na <sub>2</sub> O	0.57	0.73	0.81	0.44	1.16	1.36	1
Total	101.35	99.03	99.55	99.53	101.38	100.24	99.63
xMg	83.44	84.41	90.75	85.66	86.97	85.09	88.14
Ti / Eu	8962.34	4255.83	1392.63	1675.24	1564.57	632.76	796.80
Sc	100.2	68.2	43.5	99.6	56.7	33.8	72.2
Ti	9416	3564	553	1596	1832	1042	827
V	287	281	169	421	196	127	175
Cr	116	3249	4586	4300	5707	2395	5231
Co	29.56	28.39	31.48	36.58	26.41	71.42	25.30
Y	7.86	7.35	3.45	10.11	14.86	23.04	9.46
Zr	89.60	33.17	7.90	27.47	18.85	54.58	40.49
Nb	0.75	0.30	0.17	0.41	1.32	1.23	0.11
La	4.46	4.37	13.77	7.78	6.94	28.32	8.50
Ce	16.34	15.23	35.10	25.50	21.76	63.45	30.37
Pr	2.80	2.57	3.89	3.90	3.23	7.28	4.62
Nd	14.53	12.92	12.09	17.54	14.51	27.02	20.75
Sm	3.57	2.89	1.58	3.30	3.16	4.73	3.79
Eu	1.05	0.84	0.40	0.95	1.17	1.65	1.04
Gd	3.21	2.62	0.97	2.76	3.24	4.71	2.86
Tb	0.35	0.32	0.09	0.37	0.48	0.66	0.37
Dy	2.09	1.68	0.62	2.02	2.95	4.20	2.00
Ho	0.33	0.29	0.12	0.40	0.59	0.86	0.35
Er	0.81	0.70	0.33	0.99	1.57	2.29	0.97
Tm	0.08	0.10	0.04	0.16	0.19	0.34	0.12
Yb	0.44	0.50	0.30	0.81	1.26	2.18	0.81
Lu	0.07	0.09	0.04	0.13	0.19	0.30	0.12
Hf	4.64	1.16	0.15	0.70	0.65	1.21	0.83
Ta	0.19	0.07	0.01	0.05	0.01	0.06	0.08

Table 2. Continued.

Sample	Baar 21	Baar14A	MFM-V	Neun-013	Neun-017	Neun-022	Neun-022
Location	Baarley	Baarley	Meerfeld	Neunkirchen	Neunkirchen	Neunkirchen	Neunkirchen
Type	Ia	PC	CAP vein	Ia	PC	PC	PC
SiO <sub>2</sub>	53.65	51.21	54.12	53.62	51.35	54.99	54.52
TiO <sub>2</sub>	0.38	1.23	0.05	0.28	1.06	0.21	0.15
Al <sub>2</sub> O <sub>3</sub>	1.94	3.54	4.02	1.9	4.64	2.11	2.57
FeO	4.18	4.61	2.69	3.15	3.48	2.82	2.77
MnO	0.32	0.13		20.88	0.2	0.17	0.06
MgO	16.47	15.51	16.38	17.75	15.76	18.22	17.84
CaO	22.62	23.83	20.17	0.31	23.31	21.53	21.47
NiO				0.97			
Na <sub>2</sub> O	1.12	0.6	1.5	0.31	0.73	0.97	0.99
Total	100.68	100.66	98.93	99.17	100.53	101.02	100.37
xMg	87.01	85.13	91.56	90.56	88.51	91.66	91.64
Ti / Eu	617.65	4635.08	365.13	1078.18	2582.59	7669.21	828.52
Sc	31.1	62.3	66.8	77.1	64.9	89.9	61.2
Ti	1495	5479	830	720	3865	7937	1465
V	238	190	210	295	275	232	227
Cr	5945	2765	7028	11 418	7939	1966	10 853
Co	18.48	24.03	21.00	24.42	21.07	28.14	21.29
Ni			305.43				
Sr			282.98				
Y	18.36	9.11	18.70	6.55	13.47	7.79	15.53
Zr	196.50	108.31	58.86	2.93	43.37	61.78	14.57
Nb	1.67	0.56	1.45	0.14	1.15	0.53	0.42
La	10.72	5.35	17.06	8.22	8.70	4.46	10.20
Ce	44.73	18.84	57.26	20.62	25.10	15.62	39.12
Pr	7.83	3.21	8.77	2.82	4.51	2.65	6.26
Nd	38.43	16.20	40.26	11.86	20.34	13.84	29.26
Sm	8.15	3.96	8.42	2.00	4.25	3.25	6.12
Eu	2.42	1.18	2.27	0.67	1.50	1.03	1.77
Gd	6.60	3.46	5.84	1.34	3.98	3.05	4.96
Tb	0.84	0.41	0.81	0.20	0.51	0.36	0.61
Dy	4.51	2.20	4.19	1.19	3.08	2.01	3.56
Ho	0.79	0.39	0.82	0.27	0.59	0.36	0.61
Er	2.07	0.95	1.56	0.72	1.38	0.88	1.61
Tm	0.27	0.11	0.25	0.10	0.18	0.08	0.21
Yb	1.29	0.59	1.70	0.77	1.00	0.53	1.25
Lu	0.20	0.09	0.21	0.10	0.15	0.07	0.18
Hf	4.68	4.39	1.28	0.14	1.69	3.00	0.34
Ta	0.33	0.17	0.16		0.13	0.09	0.05

Table 2. Continued.

Sample	Neun-023	Neun-023	Neun-033	Neun-033	Rud-3	Rud-3	Rud-7
Location	Neunkirchen	Neunkirchen	Neunkirchen	Neunkirchen	Ruderbusch	Ruderbusch	Ruderbusch
Type	PC	Ia	PC	Ia	PC	PC	PC
SiO <sub>2</sub>	53.01	53.5	53.48	54.19	49.05	49.05	51.29
TiO <sub>2</sub>	0.32	0.23	0.27	0.24	1.48	1.48	0.73
Al <sub>2</sub> O <sub>3</sub>	3.51	2.21	1.89	1.49	3.91	3.91	4.68
FeO	3.2	3.05	3	2.83	4.68	4.68	3.19
MnO	0.07	0.37	0.19	0.21	0.14	0.14	0.25
MgO	16.92	18.06	17.11	17.72	14.86	14.86	16.2
CaO	21.81	20.87	21.12	23.2	23.87	23.87	23.7
Na <sub>2</sub> O	0.92	0.92	1.08	0.95	0.4	0.4	0.61
Total	99.76	99.21	98.14	100.83	98.39	98.39	100.65
xMg	89.99	90.97	91.05	91.42	84.38	84.38	89.63
Ti / Eu	3373.97	1452.74	3789.64	866.65	7205.07	8235.16	2266.49
Sc	108.57	78.11	94.57	76.92	79.60	146.76	114.68
Ti	2205.32	631.26	4660.96	1360.29	8487.44	13 582.45	2222.35
V	306.76	308.32	264.22	278.43	283.25	176.42	317.08
Cr	9502.70	12 438.21	7469.95	10 712.69	146.78	2709.77	11 710.32
Co	25.84	26.38	23.19	23.18	33.56	24.38	19.55
Ni			112.24	5.38	1.67	2.28	6.04
Rb			15.88	12.69	24.65	17.86	6.94
Y	5.99	5.07	12.10	17.28	8.47	10.99	11.78
Zr	10.40	2.16	28.95	7.18	100.63	193.92	9.55
Nb	0.08	0.04	1.44	0.37	0.72	5.26	0.96
La	4.17	10.67	9.31	14.24	5.70	11.32	10.30
Ce	13.23	26.55	28.82	45.20	19.46	35.78	32.43
Pr	1.95	2.91	4.40	6.67	3.18	5.66	4.41
Nd	9.13	9.70	20.18	30.00	16.09	26.17	17.78
Sm	2.08	1.58	4.29	5.72	3.98	5.83	3.17
Eu	0.65	0.43	1.23	1.57	1.18	1.65	0.98
Gd	1.79	1.05	3.72	4.50	3.39	4.27	2.60
Tb	0.23	0.16	0.44	0.58	0.40	0.51	0.35
Dy	1.45	0.94	2.54	3.46	2.35	2.85	2.23
Ho	0.26	0.18	0.43	0.67	0.36	0.45	0.46
Er	0.64	0.55	1.21	1.72	0.82	1.11	1.31
Tm	0.09	0.07	0.13	0.22	0.10	0.11	0.18
Yb	0.57	0.68	0.84	1.39	0.55	0.90	1.05
Lu	0.07	0.09	0.12	0.19	0.08	0.11	0.17
Hf	0.49	0.04	1.23	0.27	4.40	8.67	0.39
Ta	0.01		0.10	0.02	0.18	0.78	0.04

### 5.1.1 Clinopyroxene–amphibole–phlogopite (CAP) veins in type Ia xenoliths

Several unusual veins have been found in xenoliths from Meerfelder Maar as represented by sample MFM-V (Fig. 2a). These bright green veins, containing small patches of amphibole, are up to 15 mm wide (Fig. 2b). The host to the vein described here is an amphibole-bearing lherzolite composed of olivine, orthopyroxene, clinopyroxene, and amphibole, with very minor spinel. The grain size of olivine and orthopyroxene is between 2 and 4 mm. Amphibole and clinopyroxene are typically smaller, ranging from 1 to 2 mm. Olivine shows well-developed deformation lamellae. Phlogopite is absent

from the host, though it is present in other xenoliths with similar petrographic characteristics.

The CAP vein shows sharp but irregular contacts with the host peridotite (Fig. 2a). It comprises clinopyroxene and amphibole, with lesser amounts of orthopyroxene and olivine and, in a localized domain, phlogopite. Amphibole and clinopyroxene in the vein are typically 2–4 mm in size. Olivine occurs in several small patches; orthopyroxene is more abundant than olivine and forms rafts within the vein that are ~10 mm long. Within these rafts, amphibole occurs as an interstitial phase. Clinopyroxene is the dominant vein

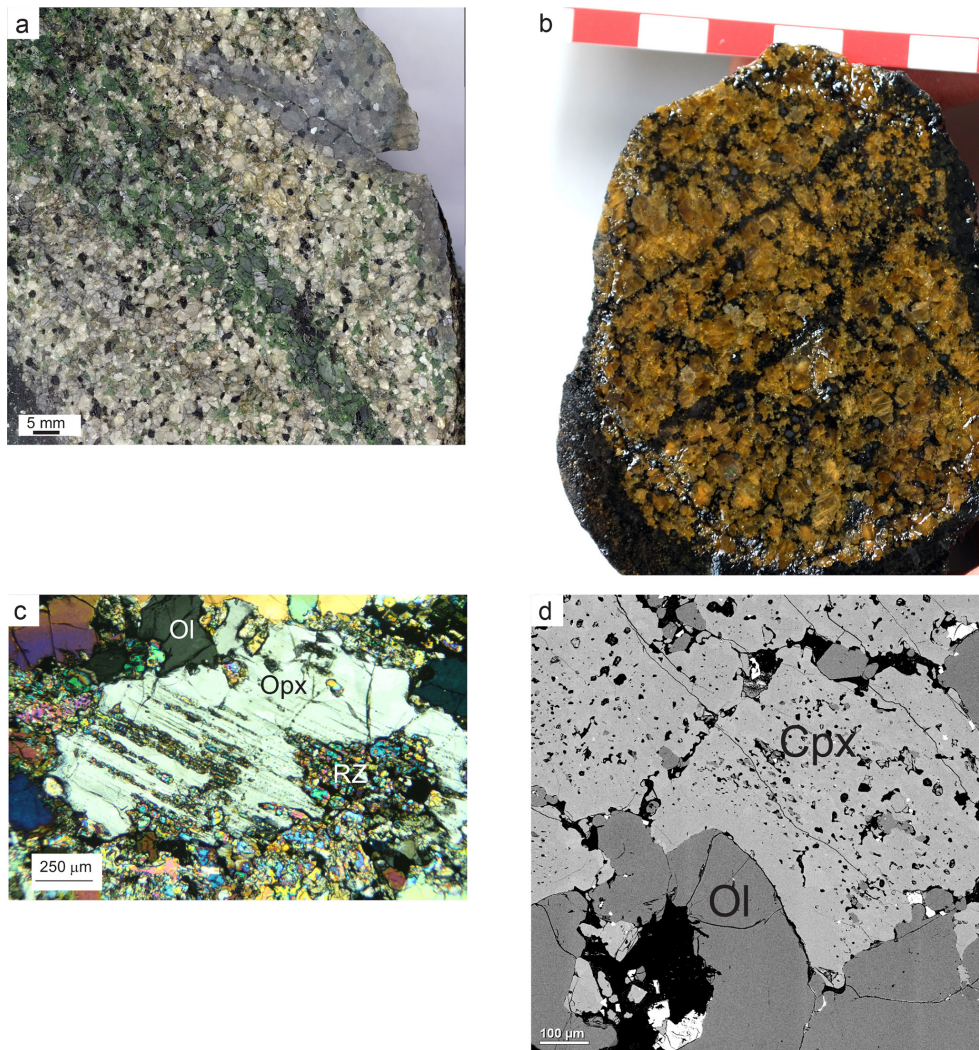


**Figure 2.** (a) Clinopyroxene–amphibole–phlogopite (CAP) vein from Meerfelder Maar. (b) Veined wehrlite xenolith (SEL1) from Rockeskyllerkopf containing phlogopite–clinopyroxene (PC) veins. (c) Typical orthopyroxene (opx) porphyroclast in a type Ib xenolith from Meerfelder Maar (96-MF-22a) showing partial replacement by olivine and clinopyroxene in a reaction zone (RZ) (plane-polarized light). (d) Sieve-textured clinopyroxene in a type Ib xenolith from Ruderbusch (Rud-7, backscattered electron image).

mineral. It is intergrown with amphibole and forms domains within the veins.

### 5.1.2 Hornblendite veins in type Ia xenoliths

Witt-Eickschen et al. (1998) described veins of amphibole that range in size from 0.1–1.2 cm in amphibole-bearing lherzolite and harzburgite. These have been reported only from Meerfelder Maar. There is commonly a 0.5–1 cm wide zone of amphibole enrichment at the vein–peridotite host contact.

### 5.1.3 Phlogopite–clinopyroxene (PC) veins in type Ia peridotite

Phlogopite–clinopyroxenite veins hosted in hydrous lherzolite and harzburgite have been found at Rockeskyllerkopf,

Baarley, Gees (Shaw et al., 2005, 2018), and Neunkirchen, a previously unstudied locality. The PC veins range in thickness from a few millimetres to more than 1 cm and occur both as through-going veins and as selvages on xenoliths. The veins and selvages commonly have marginal zones of wehrlite at the contact with the host. The veins and their host xenoliths have been described in detail by Shaw et al. (2005, 2018), who suggested that they are closely related to the hornblendites that occur at Meerfelder Maar.

## 5.2 Type Ib (anhydrous) xenoliths

These are rare, except at Dreiser Weiher and Meerfelder Maar (Fig. 1), and the samples discussed here are all from the literature (Table 1). Stosch and Seck (1980) described dunite,

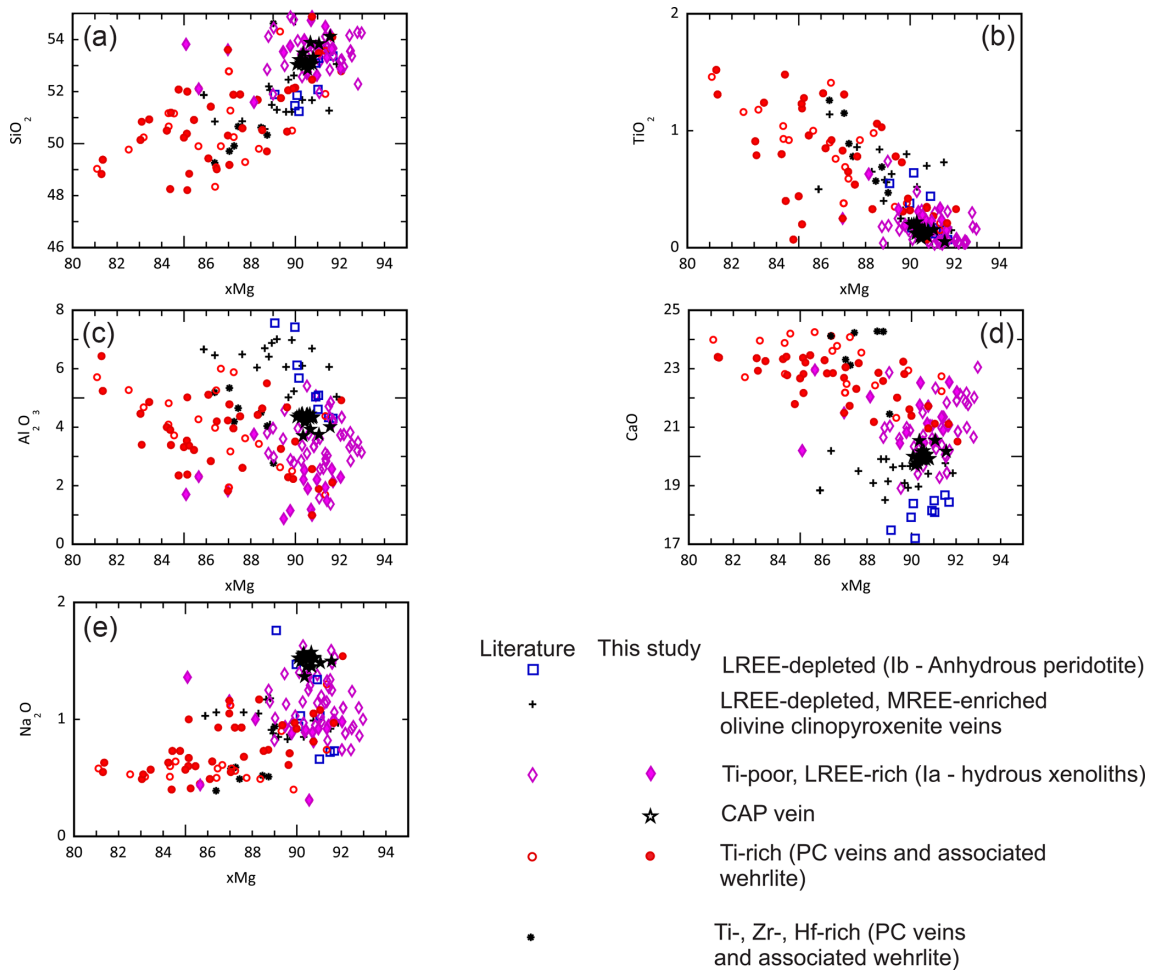


**Figure 3.** Major element composition of clinopyroxene in the West Eifel mantle xenoliths. Sources of literature data are given in Table S1. (a) xMg vs. SiO<sub>2</sub>, (b) xMg vs. TiO<sub>2</sub>, (c) xMg vs. Al<sub>2</sub>O<sub>3</sub>, (d) xMg vs. CaO, (e) xMg vs. Na<sub>2</sub>O.

Iherzolite, harzburgite, and wehrlite xenoliths as belonging to this group. Stosch and Lugmair (1986) described these rocks as coarse/protogranular, with some samples showing partial recrystallization. Xenoliths of this type from Dreiser Weiher host the olivine–clinopyroxenite veins described by Witt-Eickschen and Kramm (1998).

#### Olivine–clinopyroxenite veins in type Ib xenoliths

Witt-Eickschen and Kramm (1998) described 1–5 cm veins that cross-cut anhydrous peridotite xenoliths at Dreiser Weiher. The veins range from olivine–clinopyroxenite to monomineralic clinopyroxenite. They contain variable amounts of titanium-rich phlogopite. The contact between the veins and host is sharp and is often marked by a wehrlite zone up to 2 cm thick.

## 6 Mineral chemistry

### 6.1 Clinopyroxene

Three distinct clinopyroxene types are identified on the basis of xenolith type, mineralogical associations, and composition. Only new analyses made during this study are included in Table 2, and a complete list of all clinopyroxene compositions used is given in Table S1.

#### 6.1.1 LREE-depleted clinopyroxene

LREE-depleted clinopyroxenes are found only in the anhydrous type Ib xenoliths. They are diopside, with xMg (molecular MgO / (MgO + FeO) × 100) ranging between 88 and 91, with most having < 0.2 wt % TiO<sub>2</sub> up to a maximum of 0.64 wt %. Al<sub>2</sub>O<sub>3</sub> ranges from 4 wt % to 7.5 wt % and increases slightly with decreasing xMg. Cr<sub>2</sub>O<sub>3</sub> is between 1 wt % and 1.7 wt %, and CaO varies between 17 wt % and 19.4 wt %. Na<sub>2</sub>O has a positive correlation with Al<sub>2</sub>O<sub>3</sub> with a maximum of 1.8 wt % (Fig. 3).

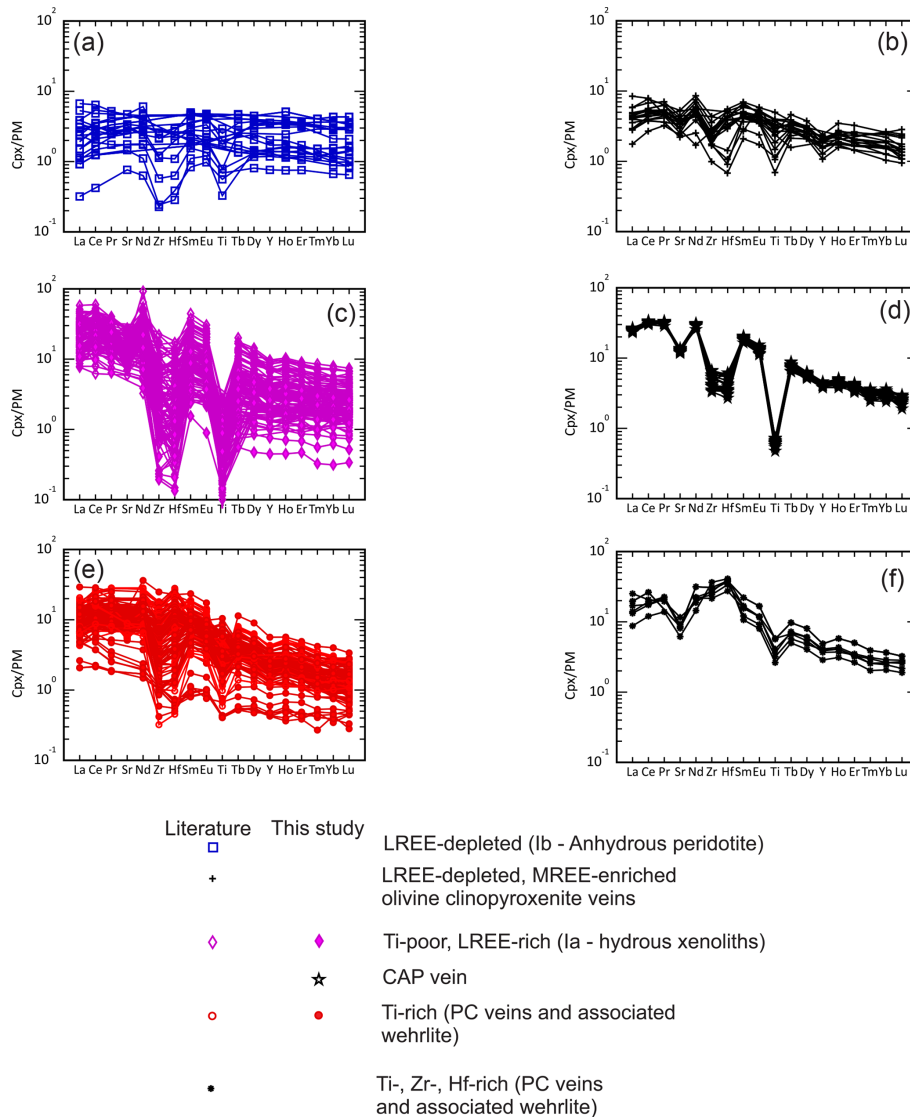


**Figure 4.** Primitive-mantle-normalized (Sun and McDonough, 1989) multi-element plots of the trace element content of clinopyroxene in the mantle peridotite xenoliths. Sources of literature data are given in Table S1. **(a)** LREE-depleted clinopyroxene from anhydrous (type Ib) xenoliths. **(b)** LREE-rich, Ti-poor clinopyroxene in olivine-clinopyroxenite veins in type Ib xenoliths. **(c)** LREE-rich, Ti-poor clinopyroxene in type Ia xenoliths. **(d)** LREE-rich, Ti-poor clinopyroxene in a clinopyroxene-amphibole-phlogopite (CAP) vein in a type Ia xenolith. **(e)** Ti-rich clinopyroxene in type Ia wehrlite xenoliths and in phlogopite-clinopyroxene (PC) veins in type Ia xenoliths with variable negative Zr and Hf anomalies. **(f)** Ti-rich clinopyroxene in type Ia wehrlite xenoliths and in phlogopite-clinopyroxene (PC) veins in type Ia xenoliths showing positive Zr and Hf anomalies.

The primitive-mantle-normalized REE patterns of clinopyroxene in the anhydrous xenoliths are flat to LREE-depleted with  $La_{(N)}$  in the range of 0.3–4, and several grains have weak negative Ti, Zr, and Hf anomalies (Fig. 4a). On a Sm/Yb vs. La/Nd plot (Fig. 5), they fall in the LREE-depleted fields, with some showing MREE depletion, but most have slight to moderate MREE enrichment.

### 6.1.2 LREE-rich, Ti-poor clinopyroxene

This type of clinopyroxene occurs in type Ia xenoliths, in the CAP vein (MFM-V) and in the wall rocks to hornblende and PC veins. It is diopside, with xMg in the range of 88–93 and low TiO<sub>2</sub> contents. It has a wider range of Al<sub>2</sub>O<sub>3</sub> content than the clinopyroxene in the anhydrous xenoliths (1 wt % to 8 wt %). Cr<sub>2</sub>O<sub>3</sub> is slightly lower, and CaO is significantly higher than in the LREE-depleted group Ib clinopyroxene (Fig. 3). The primitive-mantle-normalized trace element signatures of this type of clinopyroxene are quite different to

those of the clinopyroxene in the anhydrous peridotite xenoliths. There is strong LREE enrichment and variable but strong negative Hf, Zr, and Ti anomalies (Fig. 4b).

The CAP vein, which is hosted in a type Ia xenolith, contains diopside that shows no significant variation in major oxide composition between the vein and the host rock, with average  $xMg\# = 91.0 \pm 0.4$ ,  $TiO_2 = 0.144 \pm 0.04$  wt %, and  $Al_2O_3 = 4.11 \pm 0.38$  wt % (Table 1, Fig. 3). Diopside in the lherzolite host has negative Zr, Hf, and Ti anomalies on a primitive-mantle-normalized multi-element plot and is an LREE-enriched signature with a maximum at Ce and a steep slope down to Lu (Fig. 4d). Diopside from the CAP vein has the same La to Nd chondrite-normalized pattern and abundances as in the host but is slightly enriched in Sm to Lu, though the slope of the REE profiles is similar (Fig. 4c, d). The magnitudes of the negative anomalies for Zr, Hf, and Ti in the clinopyroxene vein are slightly smaller than those in clinopyroxene from the type Ia xenolith host (Fig. 4c, d, Table 1).

### 6.1.3 LREE-depleted, MREE-enriched clinopyroxene in olivine–clinopyroxenite veins

Diopside in these veins is similar in major element composition to the LREE-depleted clinopyroxene in the anhydrous (Ib) xenoliths but ranges to slightly lower  $xMg$  and  $Cr_2O_3$  and higher  $TiO_2$  and CaO (Fig. 3). The clinopyroxene in the host anhydrous xenoliths may show some MREE enrichment. In the veins, this type of clinopyroxene shows a small negative Zr anomaly but no Hf or Ti anomaly, whereas in the host peridotite, this type of clinopyroxene has negative Zr, Hf, and Ti anomalies (Fig. 4b).

### 6.1.4 Ti-rich clinopyroxene in phlogopite–clinopyroxene veins and wehrlite

This type of clinopyroxene is found in PC veins, wehrlite reaction zones around veins, discrete wehrlite xenoliths, and some unveined hydrous xenoliths. PC veins are absent at DW, whereas at MFM, hornblendite veins are dominated by amphibole with minor clinopyroxene. At the other locations, the veins lack amphibole and comprise variable amounts of clinopyroxene and phlogopite. This clinopyroxene type ranges in  $xMg$  from 86.5 to 92.  $TiO_2$  ranges between 0.2 wt % and 1.4 wt %; i.e., it is significantly higher than that in the xenoliths described above. CaO contents are higher for a given  $xMg$  than in the hydrous peridotites, and  $Na_2O$  contents are generally lower (Fig. 3).

There are two slightly different patterns in the primitive-mantle-normalized multi-element plot. Figure 4e shows the typical pattern, with a maximum at Ce–Pr and LREE contents between that of the anhydrous and hydrous xenolith clinopyroxene. There are very small to no negative Zr, Hf, and Ti anomalies. A small population of grains, at least one analysis from each location, except DW, shows positive

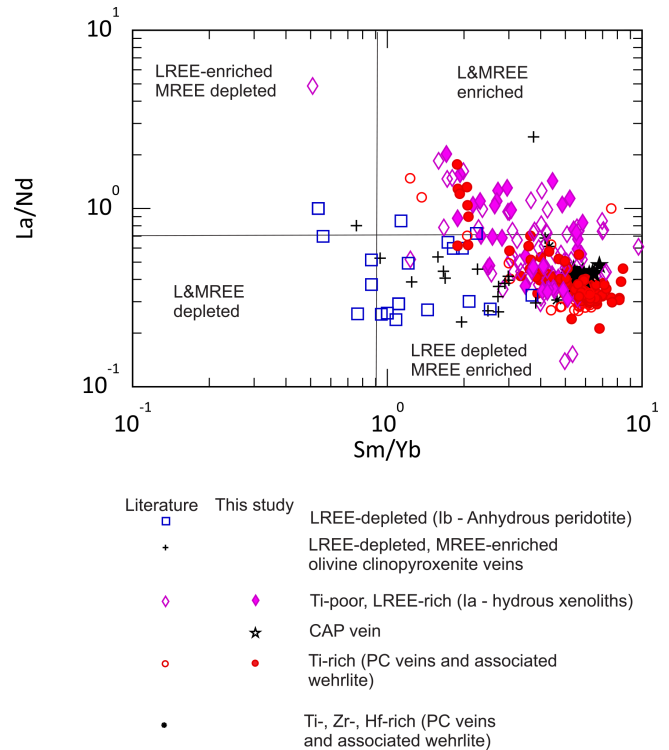


**Figure 5.** Sm/Yb vs. La/Nd plot (following Downes, 2001), showing the variety of REE patterns in clinopyroxene from the WEVF xenoliths. Sources of literature data are given in Table S1.

rather than negative or no Zr and Hf anomalies. These grains are also richer in CaO compared to the remainder of the phlogopite–clinopyroxene vein/wehrlite–clinopyroxene population.

### 6.1.5 Within-sample variations

As shown in Tables 2 and S1, each petrographic type of xenolith has a dominant clinopyroxene composition, and in most samples the clinopyroxene is homogeneous (Fig. 6a). There are several samples that show significant variation in clinopyroxene composition. Neun-23 contains two populations of clinopyroxene. The dominant population has strong negative Zr, Hf, and Ti anomalies, whereas the smaller population lacks these anomalies (Fig. 6b). There is no apparent difference in texture between the two populations. Sample 98HW1 also shows the dominant population with strong negative Zr, Hf, and Ti anomalies, but the smaller population is depleted in REE and shows only a small negative Hf and Ti anomaly (Fig. 6c). Sample 98MF1 shows a similar pattern, but in this case the differences in normalized Zr, Hf, and Ti are much smaller (Fig. 6d). Similar heterogeneity in the clinopyroxene populations is seen in xenoliths from Baarley and Neunkirchen.

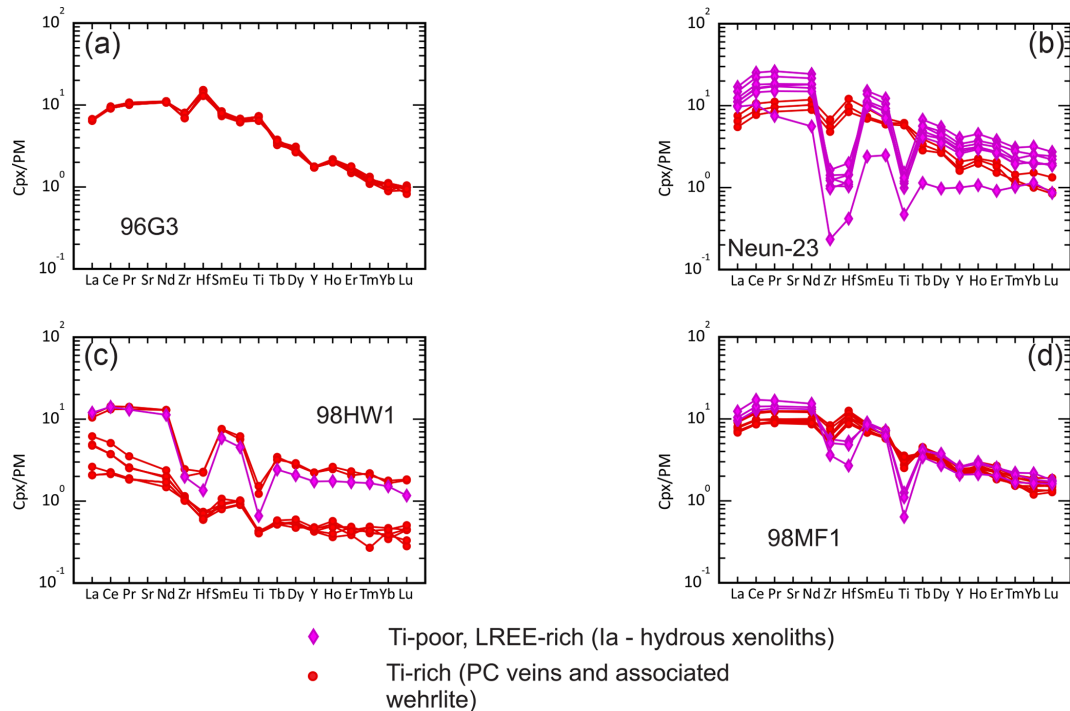


**Figure 6.** Primitive-mantle-normalized (Sun and McDonough, 1989) plots showing clinopyroxene compositional variation within individual samples. **(a)** Eight analyses from sample 96G3 showing the homogeneous character of clinopyroxene in a wehrlite xenolith. **(b)** Nine analyses from sample Neun-23 showing variable LREE and differences in the size of the negative Zr and Hf anomalies in clinopyroxene from wehrlite associated with phlogopite-clinopyroxene veins. **(c)** Seven analyses showing the variability in Ti-rich clinopyroxene in 98HW1, which has phlogopite-clinopyroxene veins hosted in wehrlite. Note that as Ti content increases, the magnitude of the negative Zr and Hf anomalies decreases. **(d)** Seven analyses of clinopyroxene in 98MF1 showing the variability in the clinopyroxene trace element signature in type Ia xenoliths affected by some melt infiltration.

## 6.2 Amphibole

Amphibole in the hydrous (type 1a) xenoliths and in the CAP vein (MFM-V) is pargasite, with xMg from 86 to 91 and TiO<sub>2</sub> less than 1 wt %. Al<sub>2</sub>O<sub>3</sub> increases with decreasing xMg. Na<sub>2</sub>O ranges between 2.5 wt % and 3.8 wt %, and K<sub>2</sub>O is between 0.2 wt % and 1.5 wt % (Table 3, Fig. 7). A primitive-mantle-normalized multi-element plot shows that the pargasite has large negative Zr, Hf, and Ti anomalies, similar to those in the co-existing clinopyroxene (Figs. 4c, 8a).

The hornblendite veins and associated wehrlite from MFM contain Ti-pargasite that has a wider range of xMg from 81 to 90. Al<sub>2</sub>O<sub>3</sub> is lower than in amphibole from the hydrous xenoliths, as is Na<sub>2</sub>O, and K<sub>2</sub>O is higher in the Ti-pargasite from the hornblendite veins (Fig. 7f). The primitive-mantle-normalized multi-element plots of these grains show that they have a weak to absent negative Zr and Hf anomaly and either no Ti anomaly or a slight positive anomaly (Fig. 8c). There is a small population of grains in the hornblendite veins that has small positive Zr and Hf anomalies (Fig. 8d).

## 6.3 Phlogopite

Disseminated phlogopite in the hydrous xenoliths has xMg of 90–93 and < 1 wt % TiO<sub>2</sub>. In the phlogopite-clinopyroxene veins and associated wehrlites, the xMg shows a wider range from 80–90, and TiO<sub>2</sub> contents are between 3 wt % and 6 wt % (Fig. 9).

## 7 Geothermometry

A compilation of the published thermometric data (Fig. 10), determined using the two-pyroxene geothermometer of Brey and Köhler (1990), shows that the anhydrous (Ib) xenoliths have high equilibration temperatures in the range 1100 to 1290 °C, with an approximately normal distribution about the mean at 1160 °C.

The hydrous (Ia) unveined peridotites show a lower temperature range with a bimodal distribution with peaks at 960 and 1020 °C. Finally, the hornblendite and olivine-clinopyroxenite veins and associated wehrlites show a bimodal distribution with peaks at 1020 and 1170 °C, with the higher temperature reflecting the crystallization conditions of the olivine-clinopyroxenites.

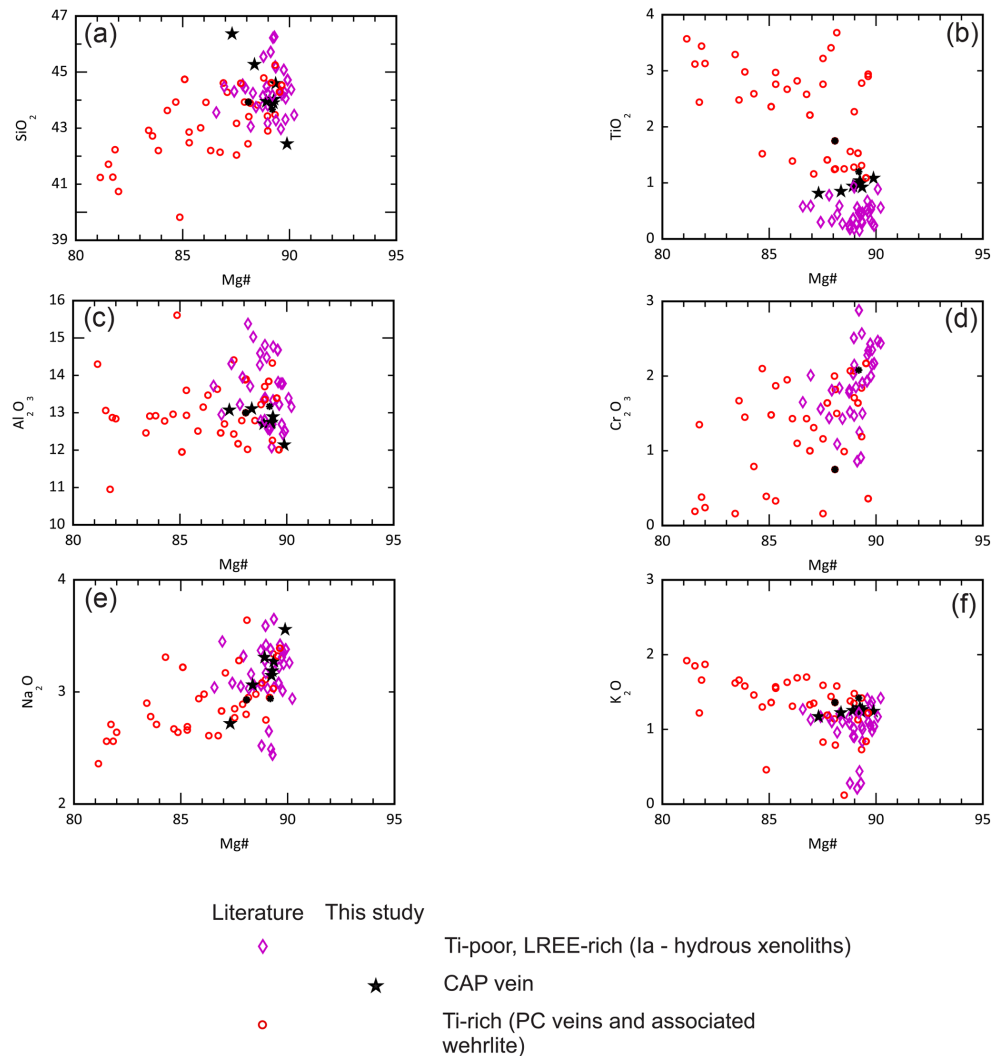


**Figure 7.** Major element composition of amphibole. Sources of literature data are given in Table S1. (a) xMg vs. SiO<sub>2</sub>, (b) xMg vs. TiO<sub>2</sub>, (c) xMg vs. Al<sub>2</sub>O<sub>3</sub>, (d) xMg vs. Cr<sub>2</sub>O<sub>3</sub>, (e) xMg vs. Na<sub>2</sub>O, (f) xMg vs. K<sub>2</sub>O.

The equilibration pressure is more difficult to estimate; however, Witt-Eickschen (2007) showed, on the basis of the Ca-in-olivine–clinopyroxene thermobarometer (Brey and Köhler, 1990), that the anhydrous xenoliths equilibrated at depths from 50–80 km, whereas the hydrous xenoliths equilibrated under slightly shallower conditions (30–50 km).

## 8 Discussion

The mineral chemical data and textural relations from this and previous studies indicate at least three events in the SCLM below the WEVF.

1. The type Ib LREE-depleted xenoliths with no MREE enrichment also show isotopic depletion (Stosch and Lugmair, 1986), both of which are indicative of partial melting of more fertile mantle. Stosch and Lug-

mair (1986) suggested that the melting event may have occurred at ~ 2 Ga.

2. In the type Ia samples and CAP vein, the Ti-poor, LREE-rich clinopyroxene, as well as the Ti-poor amphibole and phlogopite, overprint the ancient depletion. They are interpreted to be related to a mantle metasomatic event, the nature and agent of which are discussed below.
3. Clinopyroxene in olivine–clinopyroxenite veins, showing LREE depletion and MREE enrichment and no Hf and Ti anomalies, has been related by Witt-Eickschen and Kramm (1998) to the passage of primitive alkaline mafic magma that is genetically related to the Quaternary Eifel magmatism. Similarly, the Ti-rich clinopyroxene, amphibole, and phlogopite in the phlogopite–clinopyroxene veins and associated wehrlites have been



**Table 3.** Representative amphibole compositions from the clinopyroxene–amphibole–phlogopite (CAP) veins.

Sample	MFM-V						
SiO <sub>2</sub>	46.37	45.27	44.03	43.90	42.44	43.95	44.59
TiO <sub>2</sub>	0.82	0.85	0.99	1.04	1.08	0.94	0.93
Al <sub>2</sub> O <sub>3</sub>	13.07	13.11	12.75	12.72	12.14	12.70	12.89
FeO	4.08	4.11	3.82	3.82	3.84	3.92	3.76
MgO	15.70	17.45	17.77	17.72	19.05	17.61	17.63
CaO	10.23	10.47	10.82	10.75	10.82	10.80	10.68
Na <sub>2</sub> O	2.72	3.06	3.19	3.15	3.56	3.31	3.27
K <sub>2</sub> O	1.17	1.22	1.24	1.29	1.24	1.25	1.27
Total	94.15	95.54	94.60	94.39	94.17	94.49	95.03
#Mg	87.28	88.33	89.24	89.21	89.85	88.89	89.32
Sc	51.8	51.4	51.8	50.6	51.6	50.2	45.7
Ti	4544	4659	4591	4660	4640	4610	4426
V	341	344	350	347	350	341	326
Cr	10 095	10 313	10 711	10 594	10 794	10 698	10 168
Co	33.66	34.38	33.22	34.66	34.05	33.39	32.20
Ni	705	724	732	709	726	735	670
Rb	8.61	9.59	8.48	8.56	11.44	8.36	8.05
Sr	476	494	482	472	485	472	437
Y	19.42	18.92	19.90	19.50	19.14	18.33	16.46
Zr	88.22	83.96	89.37	85.70	92.57	85.67	63.24
Nb	151.18	124.68	152.29	151.53	141.18	131.10	97.52
Cs							
Ba	231.79	322.78	281.85	212.46	399.85	262.55	241.87
La	22.15	25.62	23.48	22.18	24.62	24.29	23.42
Ce	70.58	76.02	72.15	69.50	74.88	73.18	68.89
Pr	9.95	10.15	10.40	10.21	10.54	10.14	9.34
Nd	43.52	44.26	44.30	44.73	44.60	43.41	40.05
Sm	8.67	8.76	9.56	9.42	8.90	7.75	7.91
Eu	2.70	2.39	2.52	2.59	2.31	2.32	1.96
Gd	7.12	7.56	6.66	6.88	7.45	6.74	5.60
Tb	0.81	0.84	0.91	0.85	0.91	0.77	0.72
Dy	4.63	4.32	4.46	4.72	4.02	3.93	3.53
Ho	0.77	0.70	0.83	0.72	0.74	0.71	0.60
Er	1.94	2.03	2.02	1.74	1.92	1.75	1.62
Tm	0.28	0.23	0.23	0.23	0.17	0.21	0.17
Yb	1.36	1.25	1.35	1.36	1.36	1.21	1.04
Lu	0.22	0.15	0.18	0.17	0.18	0.19	0.15
Hf	2.14	1.93	2.18	2.20	1.99	1.98	1.51
Ta	4.91	3.49	4.92	5.71	3.92	3.69	2.75
Th	0.78	0.93	0.72	0.91	0.79	0.73	0.89
U	0.14	0.17	0.11	0.16	0.14	0.16	0.13

ene should have low Ti/Eu and high La<sub>N</sub>/Yb<sub>N</sub>, whereas clinopyroxene formed from silicate melt should have higher Ti but lower LREE, giving a high Ti/Eu and moderate to low La<sub>N</sub>/Yb<sub>N</sub> signature. For the WEVF, the nature of the agent of metasomatism that formed the disseminated Ti-poor minerals and the clinopyroxene–amphibole–phlogopite vein is poorly defined. Kempton et al. (1988) and Stosch and Lugmair (1986) suggested that these minerals formed during reaction of depleted mantle with low-density fluids. Thibault et al. (1992) argued that wehrlite xenoliths at Gees formed by reaction between orthopyroxene-bearing peridotite and

carbonatite melt, but this was challenged by Zinngrebe and Foley (1995), who showed that the observed major element compositional trends could be produced by reaction with a silicate melt. Witt-Eickschen et al. (2003) also suggested that the Ti-poor minerals in a single sample associated with this event could be related to carbonatite metasomatism but that there is little support from petrography and major element composition of the minerals to support such an origin.

As expected, based on previous studies (Shaw et al., 2005, 2018; Ma and Shaw, 2022), the phlogopite–clinopyroxene veins and associated xenoliths show a typical silicate-melt-

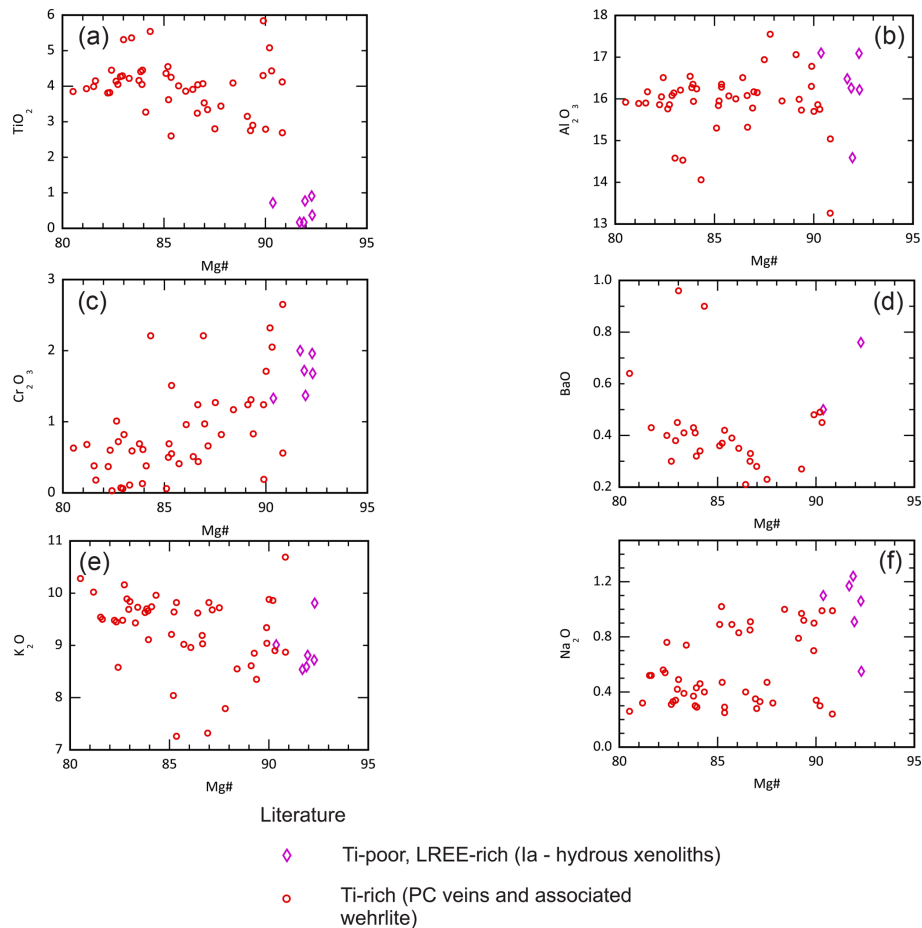


**Figure 9.** Major element composition of phlogopite. Sources of literature data are given in Table S1. (a) xMg vs.  $\text{TiO}_2$ , (b) xMg vs.  $\text{Al}_2\text{O}_3$ , (c) xMg vs.  $\text{Cr}_2\text{O}_3$ , (d) xMg vs. BaO, (e) xMg vs.  $\text{K}_2\text{O}$ , (f) xMg vs.  $\text{Na}_2\text{O}$ .

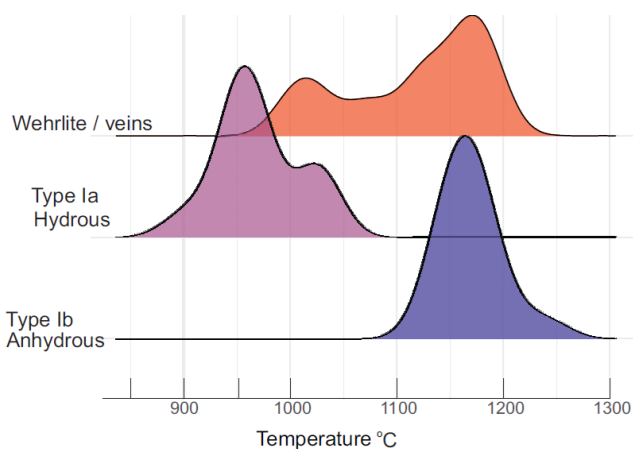


**Figure 10.** Kernel density plot of geothermometry data for WEVF xenoliths from Kempton et al. (1988), Witt-Eickschen et al. (1993), Witt-Eickschen and Kramm (1998), and Witt-Eickschen et al. (2003).

related signature, with  $\text{Ti} / \text{Eu} > 2000$  and  $\text{La}_N / \text{Yb}_N < 10$  (Fig. 11a). In contrast, the LREE-enriched, Ti-poor clinopyroxene disseminated in the hydrous xenoliths and forming the bulk of the CAP vein has  $\text{Ti} / \text{Eu} < 1700$  with  $\text{La}_N / \text{Yb}_N$  that ranges from 1 to 45. This group falls well within the field interpreted to be due to carbonatite metasomatism.

Amphibole in the melt-metasomatized xenoliths also shows high  $\text{Ti} / \text{Eu}$  and low  $\text{La}_N / \text{Yb}_N$ , whereas that in the CAP veins and type Ia xenoliths has low  $\text{Ti} / \text{Eu}$  and high  $\text{La}_N / \text{Yb}_N$  (Fig. 11b), suggesting that metasomatic amphibole may also be used in the discrimination between silicate and carbonatite metasomatism.

On the basis of the  $\text{Ti} / \text{Eu}$  and  $\text{La} / \text{Yb}$  ratios and the large negative Zr, Hf, and Ti anomalies on the primitive-mantle-normalized trace element plots, we propose that the LREE-rich, Ti-poor clinopyroxene and amphibole in the type Ia/clinopyroxene–amphibole–phlogopite (CAP) veined xenoliths are the result of interaction of depleted mantle, as represented by the type Ib xenoliths, with a carbonatite melt.

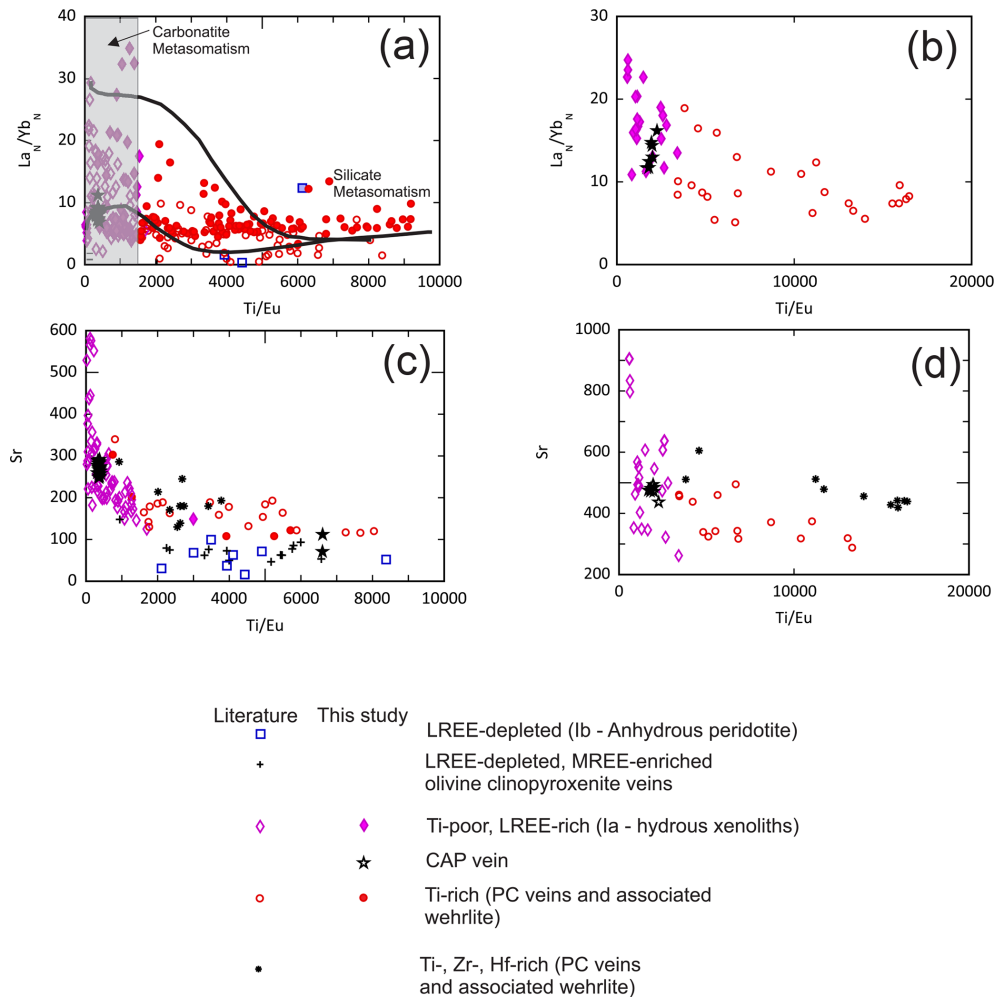


**Figure 11.** Trace element ratios and interpretation of trace element distributions of clinopyroxene and amphibole. Primitive-mantle normalization factors for La and Yb are from Sun and McDonough (1989). Sources of literature data are given in Table S1. **(a)**  $Ti/Eu$  vs.  $La_N/Yb_N$  (normalizing values from Sun and McDonough, 1989) with fields for clinopyroxene associated with silicate melt and carbonatite metasomatism (fields from Coltorti et al., 1999). The solid curves show the diffusion pathways for exchange between the composition of carbonatite-associated clinopyroxene and the composition of clinopyroxene in veins associated with silicate melt metasomatism. These profiles were calculated using the finite-difference MATLAB code from Shaw (2024). We calculated diffusion profiles using the diffusion coefficients of Ti, Eu, La, and Yb from Van Orman et al. (2001), Cherniak and Liang (2007), and Cherniak and Liang (2012). We used two different starting compositions in the models: for the carbonatite-related clinopyroxene, the grain with the highest ( $La_N/Yb_N$ ) and a grain with average ( $La_N/Yb_N$ ). For the silicate-melt-related clinopyroxene, we used the grain with the highest  $Ti/Eu$ . We calculated a diffusion profile for each element and each mineral pair using a diffusion duration of 100 000 years at 1150 °C. The element ratios were then calculated for each point in the profile and transferred to the plot. **(b)**  $Ti/Eu$  vs.  $La_N/Yb_N$  (normalizing values from Sun and McDonough, 1989) for amphibole, showing that disseminated amphibole in type Ia xenoliths and clinopyroxene–amphibole–phlogopite veins, related to carbonatite metasomatism, has low  $Ti/Eu$  and high  $La_N/Yb_N$  compared to those in hornblendite veins and associated wehrlites that are associated with silicate melt metasomatism. The carbonatite-associated amphibole has much lower  $Ti/Eu$  and  $La_N/Yb_N$  compared to amphibole in the magmatic hornblendite veins.

## 8.2 Relation of the carbonatite and silicate melt metasomatism

Although Ti-rich clinopyroxene in hornblendite/phlogopite–clinopyroxene veins and associated wehrlites can be related to metasomatism by magmas similar to those erupted in the West Eifel during the Quaternary, they also show some sim-

ilarity to the carbonatite-associated clinopyroxene, most notably in the presence of distinct negative anomalies in Zr and Hf (Fig. 4).

Petrographic data from this study and those of Witt-Eickschen et al. (1993), Witt-Eickschen and Kramm (1998), Witt-Eickschen et al. (2003), Shaw et al. (2005), and Shaw et al. (2018) indicate that the silicate metasomatic event over-

printed the carbonatite-associated metasomatism. Since Ma and Shaw (2022) used the carbonatite-metasomatized peridotite composition as their starting composition in their models, we can examine the effect of equilibration of previously metasomatized mantle with silica-undersaturated melt. The modelling indicates that at equilibrium, the silicate-metasomatized mantle should show a decrease of  $\sim 10$  in  $La_N / Yb_N$  and an increase of between 3500–6500 in  $Ti / Eu$  depending on the peridotite / melt ratio. This explains the extremes of the compositional range in the  $Ti / Eu$  vs.  $La_N / Yb_N$  plot but not in the region where  $Ti / Eu$  is between 1700–3700, which would require extremely small amounts of melt infiltration. An alternative, suggested by Shaw et al. (2018), is that the clinopyroxene in the silicate-metasomatized xenoliths is not fully equilibrated but rather records variable degrees of diffusive mixing of the original carbonatite-associated clinopyroxene and the equilibrium clinopyroxene from the silicate melt. This interpretation is also supported by the heterogeneity of trace element signatures in some samples (Fig. 6). The diffusion coefficients of  $Ti$ ,  $Eu$ ,  $La$ , and  $Yb$  (Van Orman et al., 2001; Cherniak and Liang, 2007; Cherniak and Liang, 2012) vary by up to 2 orders of magnitude such that diffusive mixing would not be linear but rather would describe a curved trend (Fig. 11a); the precise trend would depend on the initial and equilibrium clinopyroxene.

Our results show that the composition and distribution of metasomatic phases in the sub-Eifel mantle are extremely heterogeneous, with individual grains of clinopyroxene preserving evidence of overprinting of two metasomatic events over distances of a few hundred micrometres, in addition to grain-to-grain and xenolith-to-xenolith heterogeneity. Such heterogeneity has also been noted in xenoliths from the Hessian Depression and the French Massif Central (Uenver-Thiele et al., 2017; Puziewicz et al., 2025).

### 8.3 Regional implications

Volcanism in western and central Europe during the Cenozoic produced a range of mildly to highly alkaline lavas and, in some cases, carbonatites (e.g., Riley et al., 1996; Lustrino and Wilson, 2007; Valentini et al., 2010). The mantle xenoliths brought to surface in these eruptions, from the Massif Central to SW Poland, preserve evidence of multiple metasomatic events (Demény et al., 2004; Galán et al., 2008; Guzmics et al., 2008; Uenver-Thiele et al., 2017; Puziewicz et al., 2025). Similar to the xenoliths from the Eifel, the xenoliths from these sites show variable overprinting of carbonatite-associated metasomatism by silicate melt metasomatism. Although in many cases the silicate-melt-associated metasomatism is interpreted to be related to the volcanism that brought the xenoliths to surface, the origin and timing of the carbonatite metasomatism are enigmatic.

Carbonatite may be generated by near-solidus melting of carbonated peridotite (Pintér et al., 2021) or by formation of

an immiscible carbonatite from silica-undersaturated mantle-derived magma (Weidendorfer et al., 2016). We speculate that there may be a link between the carbonatite- and silicate-melt-related metasomatism of the lithospheric mantle and the volcanism that brought the xenoliths to surface. We suggest two possible scenarios. First, early formed carbonatite from near-solidus melting, which would be highly mobile (Hammouda and Laporte, 2000), could ascend and react with SCLM. Further melting in the source could generate a somewhat less mobile silicate melt, which would follow the carbonatite into the SCLM, where further reaction could occur. A second possibility is that the fractionation of carbonated silica-undersaturated magma generated immiscible carbonatite melts in the mantle. In either case, the low-volume, mobile carbonatitic melts would migrate along grain boundaries, creating a mainly pervasive metasomatism, though the vein described here indicates some channelling of melt. The larger volume of silicate melt could have been confined mainly to fractures and their immediate surroundings, creating the observed veining and associated wehrlite reaction margins that are common in the Eifel mantle samples.

## 9 Conclusions

1. Previous studies have identified LREE-depleted clinopyroxene in anhydrous xenoliths that resulted from partial melting of a more primitive precursor. The depleted peridotite left after melting was the composition on which later metasomatic events were superimposed.
2. Low  $Ti / Eu$ , high  $La_N / Yb_N$ , and the distinct negative  $Zr$  and  $Hf$  anomalies of disseminated clinopyroxene in lherzolite, harzburgite, and wehrlite xenoliths provide strong evidence that the sub-Eifel mantle experienced metasomatism by carbonatite melts. Although the metasomatic phases are mainly disseminated, the CAP vein from Meerfelder Maar indicates that there was also focused flow.
3. Silicate melt metasomatism overprinted the carbonatite metasomatism. There is evidence of an early phase of silicate metasomatism that produced olivine-clinopyroxenite veins that contain LREE-depleted, MREE-enriched clinopyroxene. Infiltration of later batches of magma produced  $Zr$ - and  $Hf$ -rich clinopyroxene that is depleted in LREE compared to the carbonatite-associated clinopyroxene. The variability in clinopyroxene compositions, particularly in the wehrlites produced by melt infiltration, indicates that equilibrium between the carbonatite-metasomatized peridotite host and infiltrating melt was not completely attained.
4. The melting event is only preserved at Dreiser Weiher and Meerfelder Maar, whereas the two metasomatic

events are regionally distributed, though there are differences in the composition of the silicate melt related to the second metasomatic event, as noted by Shaw et al. (2005). The mantle below the Eifel is heterogeneous on a hand sample scale but also on a grain-to-grain scale. Analyses of clinopyroxenes in samples from numerous locations show that they preserved complex relations of trace element signatures.

**Data availability.** All analytical results are available in Table S1 in the Supplement.

**Supplement.** The supplement related to this article is available online at <https://doi.org/10.5194/ejm-37-365-2025-supplement>.

**Author contributions.** CSJS collected the samples, BEB and SM completed petrography and electron probe analysis, and BEB and SM participated in the LA-ICPMS analyses. SM made the first interpretations of the results, which were expanded upon by BEB and CSJS. SM wrote the initial draft, with contributions by BEB and CSJS. CSJS completed the paper, and all three authors edited the final version.

**Competing interests.** At least one of the (co-)authors is a member of the editorial board of *European Journal of Mineralogy*. The peer-review process was guided by an independent editor, and the authors also have no other competing interests to declare.

**Disclaimer.** Publisher's note: Copernicus Publications remains neutral with regard to jurisdictional claims made in the text, published maps, institutional affiliations, or any other geographical representation in this paper. While Copernicus Publications makes every effort to include appropriate place names, the final responsibility lies with the authors.

**Acknowledgements.** We are grateful to Douglas Hall, Steven Cogswell, and Detlef Krauß for their assistance with electron microprobe analyses at UNB and Bayreuth. Thin-section preparation by Oskar Leitner (Bayreuth) and Calvin Nash (UNB) is greatly appreciated. We thank Brandon Boucher at UNB for sharing his expertise during the LA-ICP-MS analysis. Critical reviews by Hilary Downes and the anonymous reviewer are greatly appreciated.

**Financial support.** Part of this work was completed while Cliff S. J. Shaw was a visiting scientist at the Bayerisches Geoinstitut, University of Bayreuth, Germany. Funding for fieldwork and analysis was from an NSERC Discovery grant to Cliff S. J. Shaw. Shuai Ma (University College Cork) was supported by the Irish Research Council grant IRCLA/2022/2638 to Kate Kiseeva.

**Review statement.** This paper was edited by Didier Laporte and reviewed by Hilary Downes and one anonymous referee.

## References

- Bernstein, S., Kelemen, P. B., and Hanghøj, K.: Consistent olivine Mg# in cratonic mantle reflects Archean mantle melting to the exhaustion of orthopyroxene, *Geology*, 35, 459–462, 2007.
- Blundy, J. and Dalton, J. A.: Experimental comparison of trace element partitioning between clinopyroxene and melt in carbonate and silicate systems, and implications for mantle metasomatism, *Contrib. Mineral. Petrol.*, 139, 356–371, 2000.
- Brey, G. P. and Köhler, T.: Geothermobarometry in Four-phase lherzolites II. New thermobarometers and practical assessment of existing thermobarometers, *J. Petrol.*, 31, 1353–1378, 1990.
- Büchel, G.: Vulkanologische Karte West- und Hocheifel, Landesvermessungsamt Rheinland-Pfalz, 1994.
- Cherniak, D. J. and Liang, Y.: Rare earth element diffusion in natural enstatite, *Geochim Cosmochim. Ac.*, 71, 1324–1340, 2007.
- Cherniak, D. J. and Liang, Y.: Ti diffusion in natural pyroxene, *Geochim Cosmochim. Ac.*, 98, 31–47, 2012.
- Coltorti, M., Bonadiman, C., Hinton, R. W., Siena, F., and Upton, B. G. J.: Carbonatite metasomatism of the oceanic upper mantle: Evidence from clinopyroxenes and glasses in ultramafic xenoliths of Grande Comore, Indian Ocean, *J. Petrol.*, 40, 133–165, 1999.
- Dahm, T., Stiller, M., Mechie, J., Heimann, S., Hensch, M., Woith, H., Schmidt, B., Gabriel, G., and Weber, M.: Seismological and Geophysical Signatures of the Deep Crustal Magma Systems of the Cenozoic Volcanic Fields Beneath the Eifel, Germany, *Geochem. Geophys. Geosy.*, 21, e2020GC009062, <https://doi.org/10.1029/2020GC009062>, 2020.
- Dauria, J. M., Dupuy, C., Takherist, D., and Dostal, J.: Carbonate metasomatism in the lithospheric mantle: peridotitic xenoliths from a melilititic district of the Sahara basin, *Mineral. Petrol. Contrib. Mineral. Petrol.*, 111, 37–52, 1992.
- Demény, A., Vennemann, T. W., Hegner, E., Nagy, G., Milton, J. A., Embey-Isztin, A., Homonnay, Z., and Dobosi, G.: Trace element and C–O–Sr–Nd isotope evidence for subduction-related carbonate–silicate melts in mantle xenoliths (Pannonian Basin, Hungary), *Lithos*, 75, 89–113, 2004.
- Downes, H.: Formation and modification of the shallow Subcontinental lithospheric mantle: a review of geochemical evidence from ultramafic xenoliths suites and tectonically emplaced ultramafic massifs of western and central Europe, *J. Petrol.*, 42, 233–250, 2001.
- Eickhoff, D., Ritter, J. R. R., Hlouchek, F., and Buske, S.: Seismic Reflection Imaging of Fluid-Filled Sills in the West Eifel Volcanic Field, Germany, *Geophys. Res. Lett.*, 51, e2024GL111425, <https://doi.org/10.1029/2024GL111425>, 2024.
- Galán, G., Oliveras, V., and Paterson, B. A.: Types of metasomatism in mantle xenoliths enclosed in Neogene-Quaternary alkaline mafic lavas from Catalonia (NE Spain), *Geol. Soc. Spec. Publ.*, 293, 121–153, 2008.
- Gervasoni, F., Klemme, S., Rhohrbach, A., Grutzner, T., and Berndt, J.: Experimental constraints on mantle metasomatism caused by silicate and carbonate melts, *Lithos*, 282/283, 173–186, 2017.
- Guzmics, T., Kodolányi, J., Kovács, I., Szabó, C., Bali, E., and Ntaflous, T.: Primary carbonatite melt inclusions in apatite and in K-

- feldspar of clinopyroxene-rich mantle xenoliths hosted in lamprophyre dikes (Hungary), *Mineral. Petrol.*, 94, 225–242, 2008.
- Hammouda, T. and Laporte, D.: Ultrafast mantle impregnation by carbonatite melts, *Geology*, 28, 283–285, 2000.
- Hauzenberger, C. A., Konzett, J., Joachim-Mrosko, B., and Nguyen, H.: Pliocene to Pleistocene REE-P Metasomatism in the Subcontinental Lithosphere beneath Southeast Asia—Evidence from a Monazite- and REE-rich Apatite-bearing Peridotite Xenolith from Central Vietnam, *J. Petrol.*, 65, egae015, <https://doi.org/10.1093/petrology/egae015>, 2024.
- Ionov, D. A., Ashchepkov, I. V., Stosch, H. G., Witt, E. G., and Seck, H. A.: Garnet peridotite xenoliths from the Vitim volcanic field, Baikal region; the nature of the garnet-spinel peridotite transition zone in the continental mantle, *J. Petrol.*, 34, 1141–1175, 1993.
- Ionov, D. A., Chanefo, I., and Bodinier, J. L.: Origin of Fe-rich lherzolites and wehrlites from Tok, SE Siberia by reactive melt percolation in refractory mantle peridotites, *Contrib. Mineral. Petrol.*, 150, 335–353, 2005.
- Kempton, P. D., Harmon, R. S., Stosch, H.-G., Hoefs, J., and Hawkesworth, C. J.: Open system O-isotope behaviour and trace element enrichment in the sub-Eifel mantle, *Earth Planet. Sc. Lett.*, 89, 273–287, 1988.
- Klemme, S., van der Laan, S. R., Foley, S. F., and Guenther, D.: Experimentally determined trace element and minor element partitioning between clinopyroxene and carbonatite melt under upper mantle conditions, *Earth Planet. Sc. Lett.*, 133, 439–448, 1995.
- Lloyd, F. E. and Bailey, D. K.: Light element metasomatism of the continental mantle: The evidence and the consequences, *Phys. Chem. Earth.*, 9, 389–416, 1975.
- Lloyd, F. E., Edgar, A. D., Forsyth, D. M., and Barnett, R. L.: The paragenesis of upper-mantle xenoliths from the Quarternary volcanics south-east of Gees, West Eifel, Germany, *Mineral. Mag.*, 55, 95–122, 1991.
- Lustrino, M. and Wilson, M.: The circum-Mediterranean anorogenic Cenozoic igneous province, *Earth-Sci. Rev.*, 81, 1–65, 2007.
- Ma, S. and Shaw, C. S. J.: Vein and Wehrlite Formation in the Lithospheric Mantle Below the West Eifel Volcanic Field: Modelling the Effects of Pressure, Temperature and Peridotite/Melt Ratio on Magma-Peridotite Interaction Using pMELTS and a Melt Infiltration Experiment, *J. Petrol.*, 63, egac080, <https://doi.org/10.1093/petrology/egac080>, 2022.
- Martin, L. H. J., Schmidt, M. W., Mattsson, H. B., and Gunther, D.: Element Partitioning between Immiscible Carbonatite and Silicate Melts for Dry and H<sub>2</sub>O-bearing Systems at 1–3 GPa, *J. Petrol.*, 54, 2301–2338, 2013.
- Mertes, H. and Schmincke, H.-U.: Age Distribution of Volcanoes in the West-Eifel, *Neues Jahrb. Geol. P.-A.*, 166, 260–293, 1983.
- Mertes, H. and Schmincke, H.-U.: Mafic potassic lavas of the Quaternary West Eifel volcanic field, *Mineral. Petrol. Contrib. Mineral. Petrol.*, 89, 330–345, 1985.
- Mertz, D. F., Loehnertz, W., Nomade, S., Pereira, A., Prelevic, D., and Renne, P.: Temporal–spatial evolution of low-SiO<sub>2</sub> volcanism in the Pleistocene West Eifel volcanic field (West Germany) and relationship to upwelling asthenosphere, *J. Geodyn.*, 88, 59–79, 2015.
- Neumann, E. R., Wulff-Pedersen, E., Pearson, N. J., and Spencer, E. A.: Mantle xenoliths from Tenerife (Canary Islands): Evidence for reactions between mantle peridotites and silicic carbonatite melts inducing Ca-metasomatism, *J. Petrol.*, 43, 825–857, 2002.
- Paton, C., Hellstrom, J., Paul, B., Woodhead, J., and Hergt, J.: Iolite: Freeware for the visualisation and processing of mass spectrometric data, *J. Anal. Atom. Spectrom.*, 26, 2508–2518, 2011.
- Pintér, Z., Foley, S. F., Yaxley, G. M., Rosenthal, A., Rapp, R. P., Lanati, A. W., and Rushmer, T.: Experimental investigation of the composition of incipient melts in upper mantle peridotites in the presence of CO<sub>2</sub> and H<sub>2</sub>O, *Lithos*, 396/397, 106224, <https://doi.org/10.1016/j.lithos.2021.106224>, 2021.
- Pouchou, J. L. and Pichoir, F.: New model for quantitative x-ray microanalysis, Part I: Application to the analysis of homogeneous samples, *Rech. Aerospatiale*, 5, 13–38, 1984 (English Edition).
- Puziewicz, J., Aulbach, S., Kaczmarek, M.-A., Ntaflos, T., Matusiak-Małek, M., Ziobro-Mikrut, M., and Gerdes, A.: Multi-stage evolution of the lithospheric mantle beneath the Hessian Depression (Germany): Peridotite xenoliths from Stöpfung, *Lithos*, 494/495, 107908, <https://doi.org/10.1016/j.lithos.2024.107908>, 2025.
- Riley, T. R., Bailey, D. K., and Lloyd, F. E.: Extrusive carbonatite from the Quaternary Rockeskyll Complex, West Eifel, Germany, *Can. Mineral.*, 34, 389–401, 1996.
- Rivalenti, G., Zanetti, A., Mazzucchelli, M., Vannucci, R., and Cingolani, C. A.: Equivocal carbonatite markers in the mantle xenoliths of the Patagonia backarc: the Gobernador Gregores case (Santa Cruz Province, Argentina), *Mineral. Petrol. Contrib. Mineral. Petrol.*, 147, 647–670, 2004.
- Rizzo, A. L., Faccini, B., Casetta, F., Faccincani, L., Ntaflos, T., Italiano, F., and Coltorti, M.: Melting and metasomatism in West Eifel and Siebengebirge Sub-Continental Lithospheric Mantle: Evidence from concentrations of volatiles in fluid inclusions and petrology of ultramafic xenoliths, *Chem. Geol.*, 581, 120400, <https://doi.org/10.1016/j.chemgeo.2021.120400>, 2021.
- Rudnick, R. L., McDonough, W. F., and Chappell, B. W.: Carbonatite metasomatism in the northern Tanzanian mantle: petrographic and geochemical characteristics, *Earth Planet. Sc. Lett.*, 114, 463–475, 1993.
- Schiano, P., Clocchiatti, R., Shimizu, N., Weis, D., and Mattielli, N.: Cogenetic silica-rich and carbonate-rich melts trapped in mantle minerals in Kerguelen ultramafic xenoliths: Implications for metasomatism in the oceanic upper mantle, *Earth Planet. Sc. Lett.*, 123, 167–178, 1994.
- Shaw, C. S. J.: Dissolution of orthopyroxene in basanitic magma between 0.4 and 2 GPa: further implications for the origin of Si-rich alkaline glass inclusions in mantle xenoliths, *Contrib. Mineral. Petrol.*, 135, 114–132, 1999.
- Shaw, C. S. J.: Clinopyroxenite xenoliths record magma transport and crystallization in the middle and upper Crust: A case study from the Rockeskyllerkopf Volcanic Complex, West Eifel, Germany, *J. Petrol.*, 65, egae035, <https://doi.org/10.1093/petrology/egae035>, 2024.
- Shaw, C. S. J. and Klügel, A.: The pressure and temperature conditions and timing of glass formation in mantle-derived xenoliths from Baarley, West Eifel, Germany: the case for amphibole breakdown, lava infiltration and mineral–melt reaction, *Mineral. Petrol.*, 74, 163–187, 2002.
- Shaw, C. S. J. and Woodland, A. B.: The role of magma mixing in the petrogenesis of mafic alkaline lavas, *Rockeskyllerkopf Vol-*

- canic Complex, West Eifel, Germany, *B. Volcanol.*, 74, 359–376, 2011.
- Shaw, C. S. J., Eyzaguirre, J., Fryer, B. J., and Gagnon, J.: Regional Variations in the Mineralogy of Metasomatic Assemblages in Mantle Xenoliths from the West Eifel Volcanic Field, Germany, *J. Petrol.*, 46, 945–972, 2005.
- Shaw, C. S. J., Lebert, B. S., and Woodland, A. B.: Thermodynamic Modelling of Mantle–Melt Interaction Evidenced by Veined Wehrlite Xenoliths from the Rockeskyllerkopf Volcanic Complex, West Eifel Volcanic Field, Germany, *J. Petrol.*, 59, 59–86, 2018.
- Stosch, H. G. and Lugmair, G. W.: Trace element and Sr and Nd isotope geochemistry of peridotite xenoliths from the Eifel (West Germany) and their bearing on the evolution of the subcontinental mantle, *Earth Planet. Sc. Lett.*, 80, 281–298, 1986.
- Stosch, H.-G. and Seck, H. A.: Geochemistry and mineralogy of two spinel peridotite suites from Dreiser Weiher, West Germany, *Geochim Cosmochim. Ac.*, 44, 457–470, 1980.
- Sun, S. S. and McDonough, W. F.: Chemical and isotopic systematics of oceanic basalts: implications for mantle composition and processes, *Geol. Soc. Spec. Publ.*, 42, 313–345, 1989.
- Thibault, Y., Edgar, A. D., and Lloyd, F. E.: Experimental investigation of melts from a carbonated phlogopite lherzolite; implications for metasomatism in the continental lithospheric mantle, *Am. Mineral.*, 77, 784–794, 1992.
- Tursack, E. and Liang, Y.: A comparative study of melt-rock reactions in the mantle: laboratory dissolution experiments and geological field observations, *Mineral. Petrol. Contrib. Mineral. Petrol.*, 163, 861–876, 2012.
- Uenver-Thiele, L., Woodland, A. B., Seitz, H.-M., Downes, H., and Altherr, R.: Metasomatic Processes Revealed by Trace Element and Redox Signatures of the Lithospheric Mantle Beneath the Massif Central, France, *J. Petrol.*, 58, 395–422, 2017.
- Valentini, L., Moore, K. R., and Chazot, G.: Unravelling carbonatite–silicate magma interaction dynamics: A case study from the Velay province (Massif Central, France), *Lithos*, 116, 53–64, 2010.
- Van Orman, J. A., Grove, T. L., and Shimizu, N.: Rare earth element diffusion in diopside: influence of temperature, pressure, and ionic radius, and an elastic model for diffusion in silicates, *Contrib. Mineral. Petrol.*, 141, 687–703, 2001.
- Wang, Z.-Z., Liu, S.-A., Chen, L.-H., Li, S.-G., and Zeng, G.: Compositional transition in natural alkaline lavas through silica-undersaturated melt–lithosphere interaction, *Geology*, 46, 771–774, 2018.
- Weidendorfer, D., Schmidt, M. W., and Mattsson, H. B.: Fractional crystallization of Si-undersaturated alkaline magmas leading to unmixing of carbonatites on Brava Island (Cape Verde) and a general model of carbonatite genesis in alkaline magma suites, *Contrib. Mineral. Petrol.*, 171, 43, <https://doi.org/10.1007/s00410-016-1249-5>, 2016.
- Witt-Eickschen, G. and Kramm, U.: Evidence for the multiple stage evolution of the subcontinental lithospheric mantle beneath the Eifel (Germany) from pyroxenite and composite pyroxenite/peridotite xenoliths, *Contrib. Mineral. Petrol.*, 131, 258–272, 1998.
- Witt-Eickschen, G., Seck, H. A., and Reys, C.: Multiple enrichment processes and their relationships in the subcrustal lithosphere beneath the Eifel (Germany), *J. Petrol.*, 34, 1–22, 1993.
- Witt-Eickschen, G., Kaminsky, W., Kramm, U., and Harte, B.: The nature of young vein metasomatism in the lithosphere of the West Eifel (Germany): Geochemical and Isotopic constraints from the composite mantle xenoliths from the Meerfelder Maar, *J. Petrol.*, 39, 155–185, 1998.
- Witt-Eickschen, G., Seck, H. A., Mezger, K., Eggins, S. M., and Altherr, R.: Lithospheric mantle evolution beneath the Eifel (Germany): Constraints from Sr–Nd–Pb isotopes and trace element abundances in spinel peridotite and pyroxenite xenoliths, *J. Petrol.*, 44, 1077–1095, 2003.
- Witt-Eickschen, G.: Thermal and Geochemical Evolution of the Shallow Subcontinental Lithospheric Mantle Beneath the Eifel: Constraints from Mantle Xenoliths, a Review, in: *Mantle Plumes: A multidisciplinary approach*, edited by: Ritter, J. R. R. and Christensen, U., Springer, Berlin, 323–337, ISBN 978-3-540-68046-8, 2007.
- Yaxley, G. M., Crawford, A. J., and Green, D. H.: Evidence for carbonatite metasomatism in spinel peridotite xenoliths from western Victoria, Australia, *Earth Planet. Sc. Lett.*, 107, 305–317, 1991.
- Yaxley, G. M., Green, D., and Kamenetsky, V. S.: Carbonatite Metasomatism in the Southeastern Australian Lithosphere, *J. Petrol.*, 39, 1917–1930, 1998.
- Zindler, A. and Hart, S.: Chemical geodynamics, *Ann. Rev. Earth Pl. Sc.*, 14, 493–571, 1986.
- Zinngrebe, E. and Foley, S. F.: Metasomatism in mantle xenoliths from Gees, West Eifel, Germany: evidence of calc-alkaline glasses and metasomatic Ca-enrichment, *Contrib. Mineral. Petrol.*, 122, 79–96, 1995.
- Zolitschka, B., Negendank, J., and Lottermoser, B.: Sedimentological proof and dating of the early Holocene volcanic eruption of Ulmener Maar (Vulkaneifel, Germany), *Geol. Rund.*, 84, 213–219, 1995.